PAPER

Check for updates

Magnetic properties of on-surface synthesized single-ion molecular magnets†

Katharina Diller, ‡[a] Aparajita Singha,‡[ab] Marina Pivetta, [a] Christian Wäckerlin, [ac] Raphael Hellwig,[d] Alberto Verdini,[e] Albano Cossaro, [e] Luca Floreano, [e] Emilio Vélez-Fort,[f] Jan Dreiser, [g] Stefano Rusponi [a] and Harald Brune [*a]

We perform *on-surface* synthesis of single-ion molecular magnets on an Ag(111) surface and characterize their morphology, chemistry, and magnetism. The first molecule we synthesize is $TbPc_2$ to enable comparison with chemically synthesized and subsequently surface adsorbed species. We demonstrate the formation of $TbPc_2$ with a yield close to 100% and show that on-surface synthesis leads to identical magnetic and morphological properties compared to the previously studied chemically synthesized species. Moreover, exposure of the surface adsorbed $TbPc_2$ molecules to air does not modify their magnetic and morphological properties. To demonstrate the versatility of our approach, we synthesize novel Tb double deckers using *tert*-butyl-substituted phthalocyanine (tbu-2H-Pc). The $Tb(tbu-Pc)_2$ molecules exhibit magnetic hysteresis and therefore are the first purely *on-surface* synthesized single ion magnet.

Introduction

Single molecule magnets (SMMs), and in particular single-ion magnets (SIMs), *i.e.* molecular complexes hosting a single magnetic atom, are promising building blocks for molecular spintronics applications. Lanthanide-based SIMs have been considered as prototypes for bits in high-density magnetic data storage devices and in quantum information processing.[1–10] Exploiting the SIMs in devices requires contacting them with an electrode, while preserving the stable spin orientation and long spin coherence time. Typically, SMMs are synthesized in solution by chemical means (hereafter referred to as *ex vacuo* synthesized); however, transferring them onto a surface in a clean and controlled environment is often problematic. For this purpose, the most appropriate route is thermal sublimation onto the substrate of interest.[11–14] More elaborate methods are required for SMMs whose fragility prevents their thermal sublimation, for example electrospray deposition.[15,16]

An alternative approach is the *in situ* synthesis of SIMs by *on-surface* metalation. This method consists of depositing the desired magnetic atoms onto a few layers of the free-base molecular ligands directly adsorbed on the chosen substrate. *On-surface* metalation of various free-base tetrapyrrole molecules has been intensively studied in recent years, and the procedures are well known for transition metal atoms.[17–19] Depending on the element and the preparation conditions, the reaction occurs at room temperature (RT),[20] or requires annealing.[21] For the few known examples of lanthanide metalation, the requirements are less evident. For tetraphenylporphyrins (TPPs) (Er-TPP[22] and Ce-TPP,[23,24]) metalation at room temperature is controversial, while for the preparation of cerium tetraphenylporphyrin double deckers (Ce(TPP)₂), annealing to 500 K was used.[25] For these systems the occurrence of the metalation process was demonstrated, but the magnetic properties of the resulting molecules were not investigated.

Here we introduce the *on-surface* synthesis of a Tb double decker SIM, *i.e.*, bis(phthalocyaninato)terbium(III) ($TbPc_2$).[1,2] Room temperature (RT) deposition of Tb atoms on pristine phthalocyanines (2H-Pc) adsorbed on Ag(111) gives a yield of close to 100% $TbPc_2$. Combining X-ray photoelectron spectroscopy (XPS), X-ray absorption spectroscopy (XAS), X-ray magnetic circular dichroism (XMCD), and scanning tunneling microscopy (STM), we demonstrate that the *on-surface* synthesized $TbPc_2$ possesses identical magnetic, chemical, and morphological properties to those observed for *ex vacuo* synthesized $TbPc_2$.[8] Moreover, we demonstrate that the *on-surface* prepared $TbPc_2$ molecules are robust when exposed to ambient conditions. Finally they form large-scale ordered arrays when annealed to 570 K.

aInstitute of Physics, École polytechnique fédérale de Lausanne (EPFL), CH-1015 Lausanne, Switzerland

bCenter for Quantum Nanoscience, Institute for Basic Science (IBS), Seoul 03760, Republic of Korea

cEmpa, Swiss Federal Laboratories for Materials Science and Technology, 8600 Dübendorf, Switzerland

dPhysik Department, Technische Universität München, D-85748 Garching, Germany

eCNR-IOM, Laboratorio Nazionale TASC, I-34149 Trieste, Italy

fEuropean Synchrotron Radiation Facility, Grenoble, France

gSwiss Light Source, Paul Scherrer Institut, CH-5232 Villigen PSI, Switzerland

† Electronic supplementary information (ESI) available. See DOI: 10.1039/c9ra06803a

‡ These authors contributed equally to this work.

To demonstrate the versatility of this method, we create a novel double-decker SIM, namely Tb-(tbu-Pc)$_2$ on Ag(111), starting from tbu-2H-Pc, a Pc derivative with four bulky groups attached to the main Pc structure. We show that also this novel double-decker complex exhibits magnetic hysteresis, reminiscent of long spin relaxation times. This makes Tb-(tbu-Pc)$_2$ one of the very few SIMs discovered so far that exhibits a long spin lifetime while being directly adsorbed on a metal substrate.

Results and discussion

We deposit Tb atoms on pristine 2H-Pc molecules adsorbed on Ag(111) at RT. The most stringent test of whether we have succeeded in synthesising the TbPc$_2$ target molecule with high yield is to thoroughly characterize the magnetic properties. For this, we use low-temperature (3 K) X-ray absorption spectroscopy (XAS) and magnetic circular and linear dichroism (XMCD and XLD, see scheme in Fig. 1a), at the Tb M$_{4,5}$ edge (Fig. 1b), and compare the results with the corresponding measurements on *ex vacuo* synthesized TbPc$_2$ deposited on Ag(100) (Fig. 1c).[8] For comparison among samples with different Tb coverages, all spectra are normalized with respect to the total XAS peak area (see Methods). The substantial XMCD signal indicates the presence of a large magnetic moment at 6.8 T and 3 K. Moreover, the XMCD in normal incidence is larger than that measured in grazing incidence. This angular anisotropy, as well as the XLD signal measured at 0.05 T, evidence the flat-lying geometry of the molecules with an out-of-plane easy magnetization axis, as also reported for the case of *ex vacuo* synthesized TbPc$_2$.[8]

The XMCD and XLD measurements observed for the *on-surface* synthesized TbPc$_2$ are very similar in shape and intensity to the ones obtained for the *ex vacuo* synthesized TbPc$_2$, implying that all Tb atoms are incorporated into free-bases during the metalation reaction. Any Tb left over would form clusters on Ag(111) that have an in-plane easy axis, which would result in a overall reduced XMCD intensity, and very different multiplet features in both XAS and XMCD, see Fig. S1 (ESI†). This enables us to clearly distinguish Tb clusters from metalated molecules. Note that our XMCD and XLD spectra are very similar to the ones reported for *ex vacuo* TbPc$_2$ on Cu(100),[4] on Ag(100), MgO, h-BN/Ru(0001),[8] and on graphene/SiC(0001).[26] This shows that for these different substrates the Tb magnetic ground state is the same, and that the molecules are flat-lying. Given the strongly different electronic characters of these substrates, going from metallic to insulating, we can infer that the TbPc$_2$ hybridization with all these substrates is weak, leaving the molecules intact and essentially undistorted. This small influence of the substrate also justifies the fact that we compare the *on-surface* synthesized molecules on Ag(111) with the *ex vacuo* synthesized ones on Ag(100).

Ex vacuo synthesized TbPc$_2$ exhibits slow magnetic relaxation leading to magnetic hysteresis.[8] We perform the same measurements to verify the quality of the TbPc$_2$ prepared by *on-surface* metalation. Magnetization curves are obtained by recording the maximum of the XMCD signal at the Tb M$_5$ edge as a function of the external magnetic field (Fig. 1b lower panel). Notably our *on-surface* synthesized molecules exhibit the same
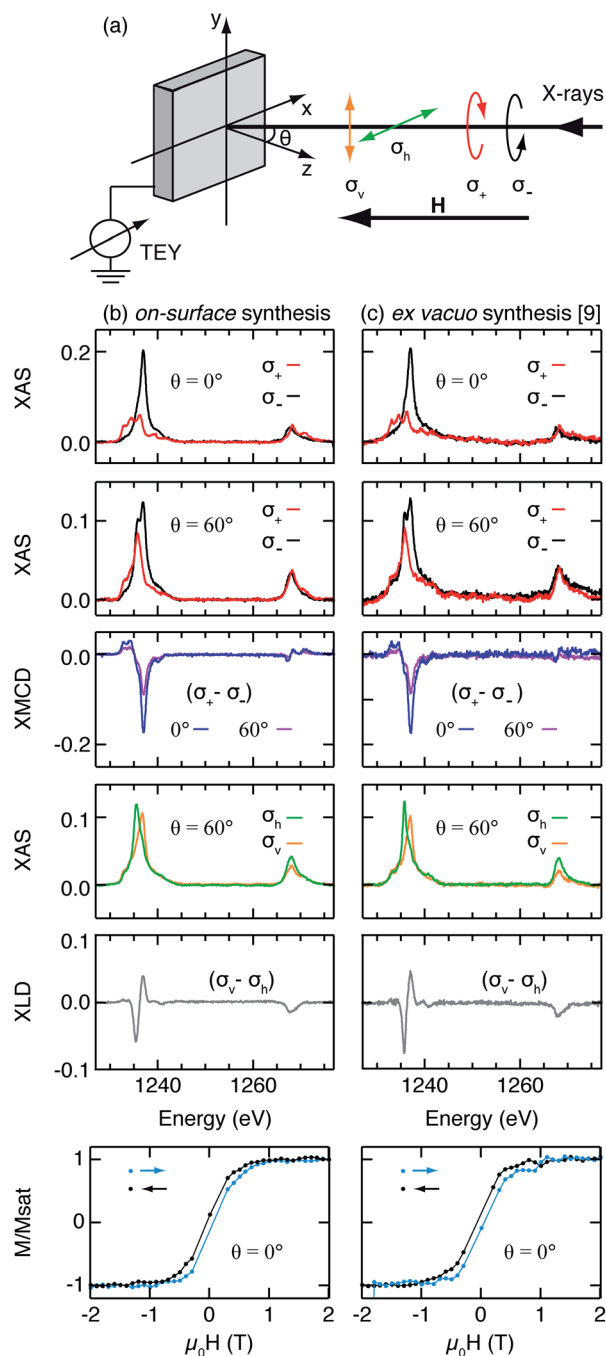

Fig. 1 (a) Schematic of the experimental geometry and the definitions of X-ray polarizations. (b) *On-surface* synthesized TbPc$_2$: XAS with circular polarizations, XMCD, XAS with linear polarizations and XLD at the Tb M$_{4,5}$ edges along with magnetization curves probed at the Tb M$_5$ edge (3.4 ML 2H-Pc/Ag(111) + 0.7 ML Tb, T_{dep} = 300 K). (c) The same for *ex vacuo* synthesized 0.3 ML TbPc$_2$/Ag(100) from ref. 8. (μ_0H = 50 mT and 6.8 T for measurements with linear and circular polarizations, respectively, $\mu_0\dot{H}$ = 2 T min^{-1} for magnetization curves measurements, T = 3 K).

magnetic hysteresis as reported for the *ex vacuo* synthesized TbPc$_2$/Ag(100) (Fig. 1c lower panel).

Further evidence for the success of the metalation reaction comes from XPS and STM measurements. Fig. 2a (upper panel) shows the N 1s XPS region measured on 1.9 ML 2H-Pc/Ag(111)
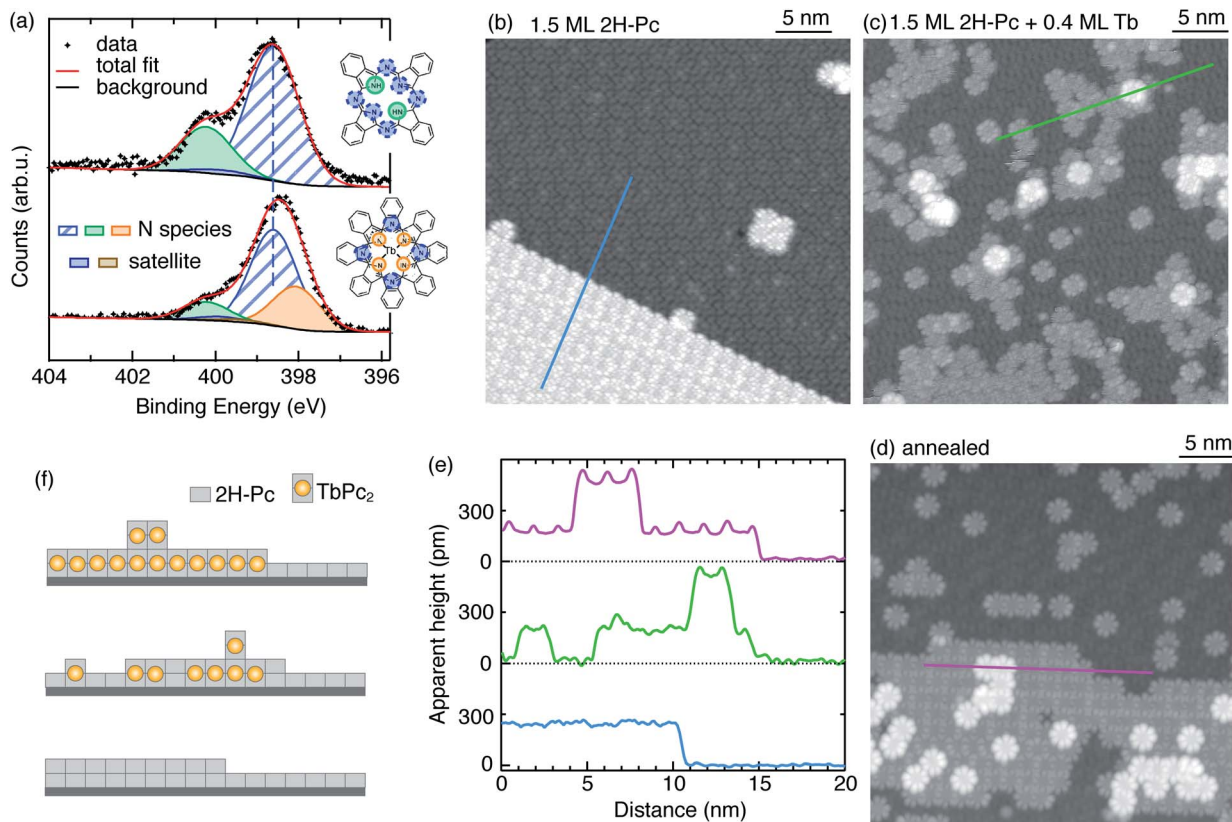
Fig. 2 (a) N 1s XPS spectra and corresponding fit for 1.9 ML pristine 2H-Pc molecules (upper panel) and after deposition of 0.5 ML Tb, yielding 0.5 ML *on-surface* synthesized TbPc$_2$ molecules (lower panel). Schematics of 2H-Pc and TbPc$_2$ are shown as insets. For the case of TbPc$_2$, only top layer N atoms are highlighted. STM image of (b) 2H-Pc ($V_t = -2.0$ V, $I_t = 20$ pA, $T = 5$ K), and (c) ≈0.4 ML *on-surface* synthesized TbPc$_2$ ($V_t = -2.0$ V, $I_t = 50$ pA, $T = 5$ K); (d) same as (c) after 15 min of annealing at 500 K ($V_t = -2.0$ V, $I_t = 50$ pA, $T = 5$ K). (e) Line profiles corresponding to the line-cuts shown in (b), (c) and (d); (f), corresponding models.

(see Methods for the ML definition). It exhibits two well separated peaks corresponding to the two differently bound N-species: –N═ (hereafter named as N for simplicity) and –NH– (that we call NH).[17,18] Peak N combines contributions from iminic (central) and aza (outer) nitrogen since their core level shifts are very similar while the one of NH is clearly different. Using Gaussian fits and constraining a 1 : 3 ratio as expected from stoichiometry for the NH to N peak intensity,[27–29] we find the energy position of the NH and N peaks at 400.2 eV and 398.6 eV, respectively (see Methods for details).

Deposition of Tb at RT leads to a reduction of the NH peak intensity and to a concomitant broadening of the main peak, see Fig. S2 (ESI†). The XPS spectrum after 0.5 ML of Tb is shown in Fig. 2a, lower panel. To fit these data, we have to introduce N–Tb as the third N-related component. Positions of NH and N peaks were kept fixed at the values found for the free-base 2H-Pc. The contribution from peak N was fixed to the total contribution from the N–Tb peak plus three times that of NH, as imposed by stoichiometry. With this constraint, we identify the N–Tb component at 398.1 eV. Its binding energy is lower than that of iminic nitrogen and it is well below the energy range for transition metal coordinated tetrapyrrole nitrogen species (*e.g.* 398.5–398.9 eV for Co-, Ni-, Cu-, and Zn-TFcP[30] and 398.7 eV for FePc[28]). This can be rationalized considering the significantly higher reactivity of lanthanides.

To gain further insights about the reaction products we perform STM measurements. At RT the free-base molecules assemble into well-ordered islands. As seen in Fig. 2b, at 1.5 ML 2H-Pc, the surface is completely covered with the first layer of free-base and extended, compact islands form in the second layer. After depositing 0.4 ML of Tb (Fig. 2c), two species with different apparent height h are observed, as shown in Fig. 2e. The predominant (gray) features have the same apparent height with respect to the free-base layer as the second-layer 2H-Pc ($h \approx 240$ pm). They exhibit the pattern typical for TbPc$_2$ consisting of eight lobes with equivalent apparent heights, at variance with the non-homogeneous contrast observed on free-base molecules in the second layer. Therefore we identify them as *on-surface* synthesized TbPc$_2$ embedded in the free-base layer (see Fig. 2f).[11,31,32] The brighter features, imaged with an apparent height of 330 pm with respect to the underlying TbPc$_2$ molecules, are attributed to second layer TbPc$_2$,[11,33,34] although formation of Tb$_2$Pc$_3$ cannot be excluded.[35,36] Combining the information obtained from XPS and STM with that from XAS, XMCD, and XLD measurements, we conclude that the metalation reaction leads to the formation of TbPc$_2$ at RT.

From experiments with varying coverages of 2H-Pc and Tb, we infer the following strategy to ensure that all Tb atoms are incorporated in the molecules: (a) a ratio of Tb to 2H-Pc smaller

than the target stoichiometry of 0.5; (b) an amount of 2H-Pc between 2 and 4 ML. This strategy leaves an excess of unreacted molecules on the surface as shown in Fig. 2. These molecules have no effect on the observed magnetic properties since the lateral magnetic interactions among TbPc$_2$ molecules are negligible.[8] Therefore slightly diluting TbPc$_2$ with unreacted molecules does not influence the observed magnetic properties. Tb in excess results in the concomitant formation of TbPc$_2$ and Tb clusters visible as bright spots in the STM images shown in Fig. S3 (ESI†). The presence of clusters is also revealed by the strong reduction of the XMCD signal acquired at normal incidence, associated with a reduction and inversion of the XLD signal, see Fig. S4 (ESI†).

The STM image in Fig. 2c shows that for RT preparation the sample morphology is quite rough and a few unreacted second layer free-base molecules coexist with reacted molecules. They are mobile under the influence of the STM tip as seen in the lower part of the image, where the molecular structure is fuzzy.

Annealing at 500 K for 15 min produces a rearrangement of the molecules leading to an increased spatial order (Fig. 2d). Note that the second layer TbPc$_2$ molecules are still present as also demonstrated by the line profile. The typical morphology after RT deposition is also evident in samples prepared with a larger amount of molecules. For a sample consisting of 2.7 ML

of 2H-Pc plus 0.8 ML of Tb, the large-scale image in Fig. 3a shows the species already identified in Fig. 2, piled into additional layers. Annealing at 570 K for 30 min leads to partial desorption of unreacted free-base molecules, to segregation of the different molecular species and to a dense, ordered packing of the TbPc$_2$. Such long-range ordering of TbPc$_2$ is evident from the middle terrace of Fig. 3b, the left terrace of Fig. 3c, and the corresponding zoom shown in Fig. 3d. In the latter image the TbPc$_2$ molecules appear with alternating bright/dark contrast.[32,33,37,38] This is even more evident in Fig. 3e showing high resolution images of the same TbPc$_2$ island acquired with two tip terminations yielding different submolecular appearances. From the orientation of the lobes and of the resulting pattern we deduce that the bright/dark contrast corresponds to a difference of about 10° in the azimuthal orientation of the molecules as highlighted by the crosses superimposed onto the molecule assembly. A tentative model of the molecular arrangement with respect to the Ag(111) surface is shown in Fig. 3f. The unit cell is a 2.02 nm-side square, yielding a molecule–molecule distance of 1.43 nm, fully compatible with already reported ordered assemblies of TbPc$_2$ molecules on surfaces.[8,33,37,38] Note that from our data we cannot conclude whether the whole molecule[38] or only the upper Pc ligand[37] is rotated.
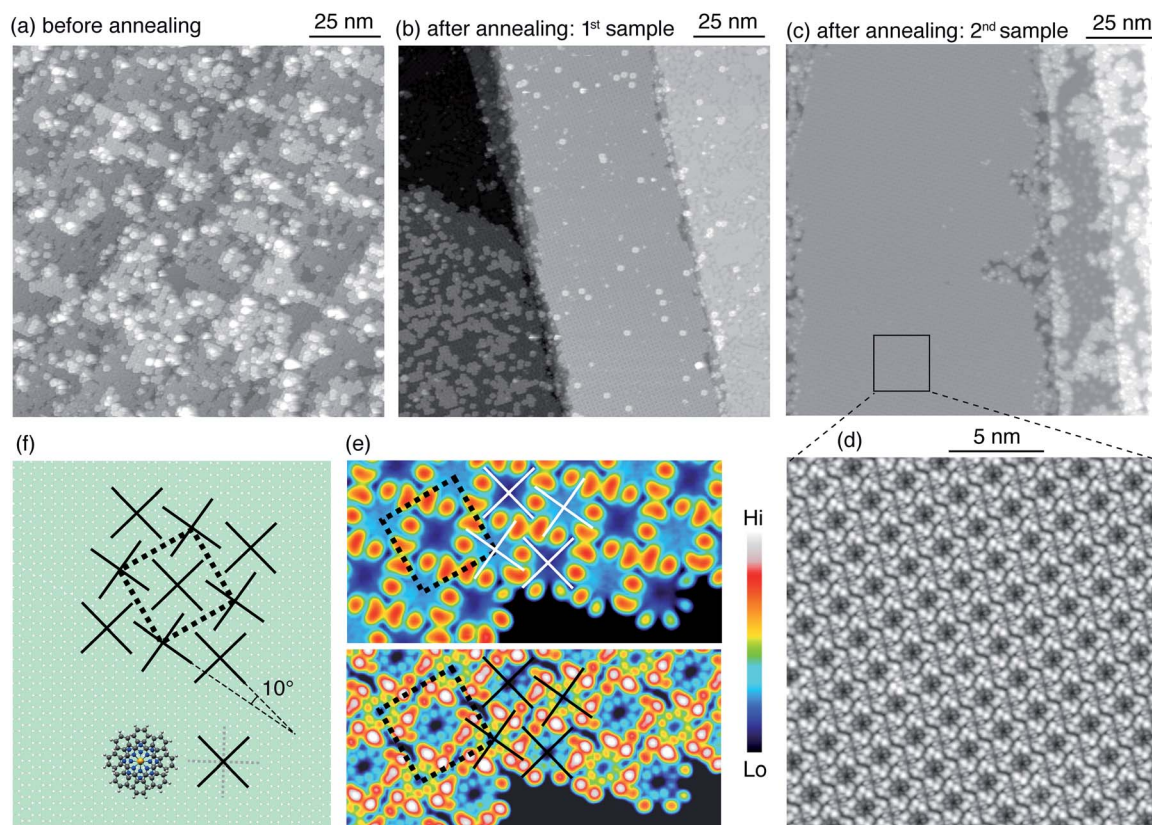

Fig. 3 (a) STM image showing irregular arrangement of *on-surface* synthesized TbPc$_2$ molecules (2.7 ML 2H-Pc/Ag(111) + 0.8 ML Tb). (b) Upon annealing at 570 K for 30 min, the TbPc$_2$ molecules organize in large ordered islands. (c) As in (b) for a different sample (2.2 ML 2H-Pc/Ag(111) + 0.8 ML Tb). (d) Zoom into the marked area in (c) showing the perfectly ordered TbPc$_2$ lattice. (e) High-resolution STM images; white and black crosses indicate the molecular orientation; unit cell is shown as a square ($V_t = -2.0$ V, $I_t = 20$ pA, $T = 5$ K for all panels). (f) Model showing the TbPc$_2$ packing with respect to the Ag(111) substrate.

Rare earths are very reactive. However, one of the many advantages of TbPc$_2$ comes from Tb being sandwiched between two Pc macrocycles which potentially protects it from contamination. In order to verify this in our *on-surface* synthesized TbPc$_2$, we performed XAS, XMCD, and XLD measurements on a sample before and after exposing it to ambient conditions. As demonstrated in Fig. 4a and b, the spectroscopic fingerprints, *i.e.*, the shape of the XAS profile and the amplitude of the XMCD and XLD profiles measured at the Tb $M_{4,5}$ edges, remain unmodified. Moreover, corresponding STM measurements reveal identical appearances of the molecules before and after the exposure to air, proving the chemical robustness of the *on-surface* synthesized SIMs (Fig. 4c and d).

The mere reproduction of already known compounds is not the final goal of *on-surface* metalation. Ideally, one would aim at the creation of novel molecules that were not produced by *ex vacuo* synthesis, in particular, species that are potentially difficult

to adsorb on surfaces as a whole. To prove the versatility of our approach, we create a novel double decker complex starting from a different phthalocyanine free-base. It is known that the metalation of tetrapyrrole molecules with on-top deposited metal atoms does not depend on the peripheral substituents.[17] Therefore interesting candidates are molecules with the same central macrocycle but with peripheral groups that can possibly increase the distance between magnetic atom and supporting substrate, reducing the hybridization of the metal ion with the substrate and decoupling it from substrate phonons and electrons. We chose tbu-2H-Pc as the free-base since it has four additional bulky *tert*-butyl (tbu) groups attached to the main phthalocyanine structure (Fig. 5a). Similar to the case of 2H-Pc, we deposit Tb atoms on tbu-2H-Pc directly adsorbed on Ag(111) at RT. The combined XAS and STM results presented in Fig. 5 and 6 demonstrate the formation of Tb(tbu-Pc)$_2$ molecules.

The magnetization curves in Fig. 5c evidence that this new compound also exhibits magnetic hysteresis. There are only very few SIMs that exhibit hysteresis being in direct contact with
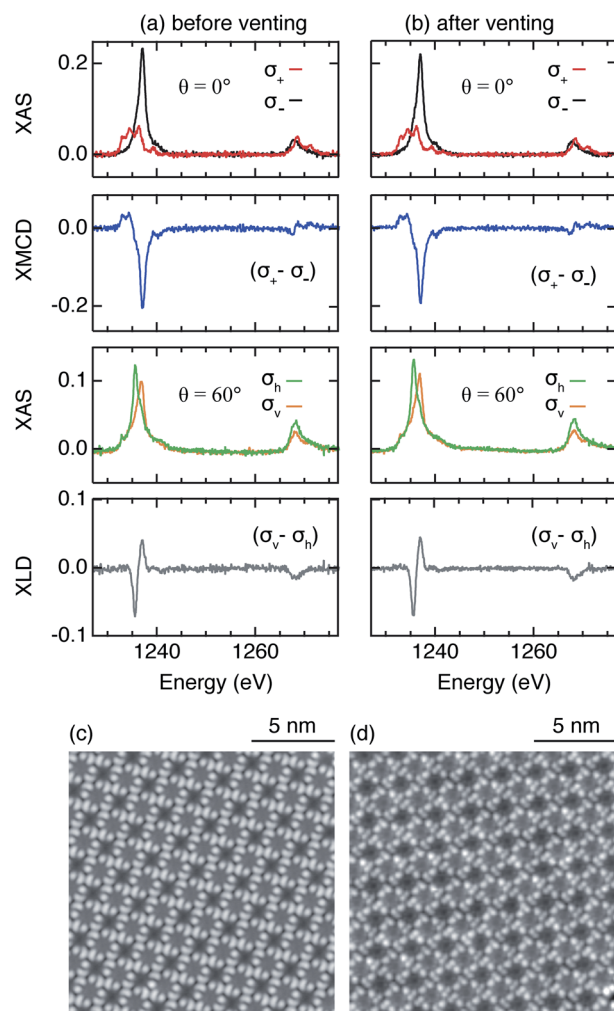

Fig. 4 XAS with circular polarizations, XMCD, XAS with linear polarizations, and XLD measured at the Tb $M_{4,5}$ edge (a) before and (b) after exposure to ambient conditions for 1 hour (2.3 ML 2H-Pc/Ag(111) + 0.4 ML Tb; $\mu_0 H = 100$ mT and 8.0 T for measurements with linear and circular polarizations, respectively, $T = 6$ K). Representative STM images are shown in (c) and (d), respectively (2.7 ML 2H-Pc/Ag(111) + 0.8 ML Tb; $V_t = -2.0$ V, $I_t = 20$ pA, $T = 5$ K).
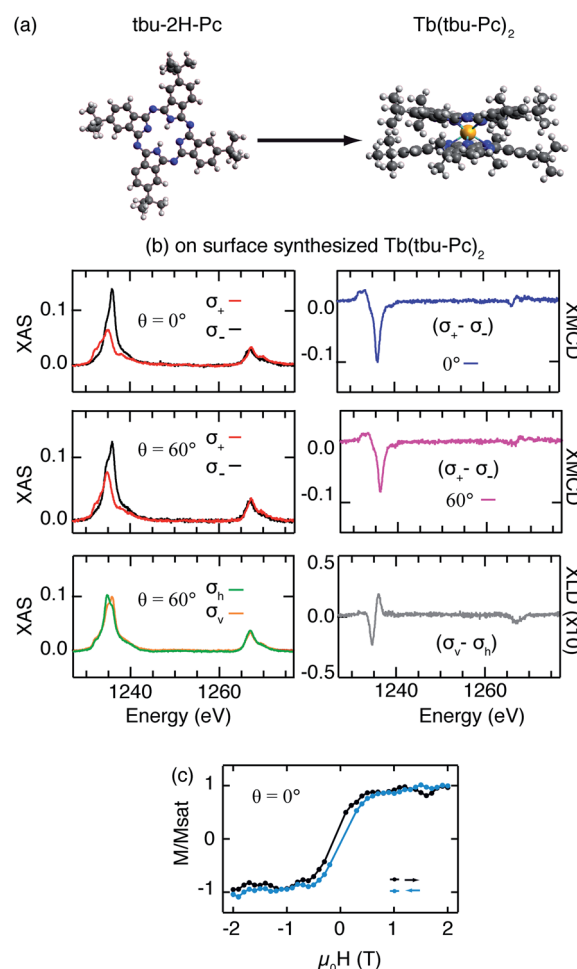

Fig. 5 (a) Schematic of tbu-2H-Pc and Tb(tbu-Pc)$_2$. (b) XAS, XMCD, and XLD probed at the Tb $M_{4,5}$ edges and (c) magnetization curve probed at the Tb M_5 edge (3.7 ML tbu-2H-Pc/Ag(111) + 0.8 ML Tb; $\mu_0 H = 50$ mT and 6.8 T for measurements with linear and circular polarizations, respectively, $\mu_0 \dot{H} = 2$ T min^{-1} for magnetization curves measurements, $T = 3$ K).
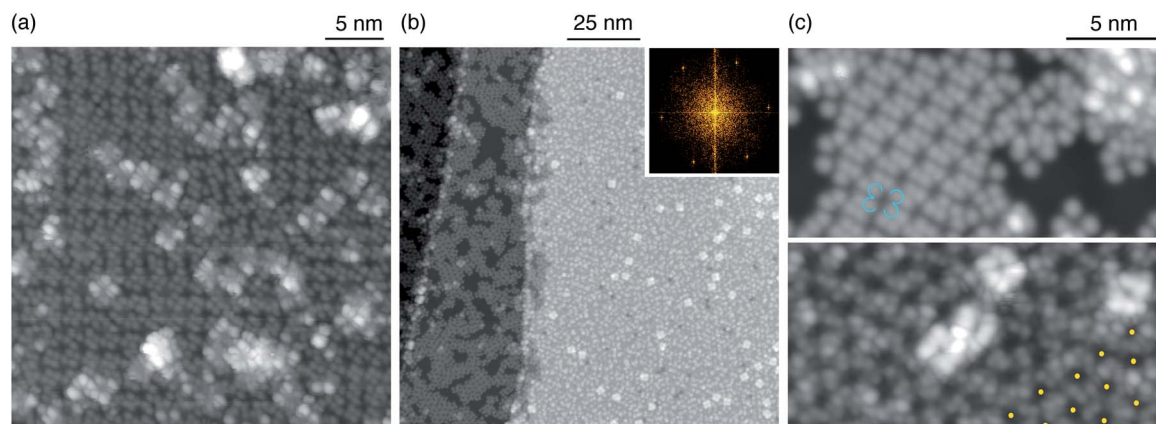
Fig. 6 STM images of (a) Tb(tbu-Pc)$_2$ embedded in a tbu-2H-Pc layer after RT deposition of Tb on tbu-2H-Pc molecules; (b) after annealing at 570 K for 30 min. Left terraces: mainly free-base molecules, right terrace: large-scale ordered islands of Tb(tbu-Pc)$_2$; (inset) FFT obtained from a region exclusively covered by Tb(tbu-Pc)$_2$. (c) High-resolution STM images of different regions of the annealed sample. Top: tbu-2H-Pc molecules; the cyan circles highlight a single tbu-2H-Pc molecule in the assembly. Bottom: Tb(tbu-Pc)$_2$ molecules; the yellow dots in the lower-right corner indicate the center of the molecules and serve as a guide to the eye. Brighter molecules are second-layer Tb(tbu-Pc)$_2$ (1.8 ML tbu-2H-Pc/Ag(111) + 0.6 ML Tb; $V_t = -2.0$ V, $I_t = 50$ pA, $T = 5$ K).

a metal surface. This newly synthesized molecule, Tb(tbu-Pc)$_2$, is one of them. The environment of the Tb atom, sandwiched between two macrocycles in both TbPc$_2$ and Tb(tbu-Pc)$_2$, generates the same crystal field thus suggesting an identical ground state for the Tb atom in the two compounds. However, in comparison with TbPc$_2$, the reduced XLD amplitude and XMCD angular anisotropy hint at a distribution of canted easy axes due to adsorption of the Tb(tbu-Pc)$_2$ molecules with a tilt angle between the macrocycles and the substrate surface. This interpretation is supported by the STM image of Fig. 6a showing randomly dispersed Tb(tbu-Pc)$_2$ molecules embedded in the tbu-2H-Pc first layer, characterized by an irregular appearance of the lobes.

Annealing at 570 K for 30 min induces segregation of the different molecular species resulting in an ordered arrangement of the Tb(tbu-Pc)$_2$ visible on the right-hand terrace in Fig. 6b, and partial desorption of the unreacted molecules (left-hand terraces). The upper panel of Fig. 6c shows a terrace partially covered by tbu-Pc molecules, each displaying four-protrusions.[39] The bottom panel of Fig. 6c shows that the Tb(tbu-Pc)$_2$ islands have a few second layer Tb(tbu-Pc)$_2$ appearing as the brightest objects, similar to the morphology observed for the annealed TbPc$_2$. The Tb(tbu-Pc)$_2$ molecules self-assemble into a hexagonal structure as evident from the FFT pattern obtained from a large scale region covered exclusively by Tb(tbu-Pc)$_2$ (inset in Fig. 6b). In Fig. 6c-bottom, the yellow dots mark the center of the molecules, revealing that the structure is not fully regular. The presence of different regioisomers of the free-base can explain this imperfect spatial order.[40] The average real space periodicity of 2.0 nm is 40% larger than the one observed for TbPc$_2$, as expected from the larger molecule size.

Summary and conclusions

We combined X-ray photoemission and absorption spectroscopy with scanning tunnelling microscopy to show the

successful *on-surface* synthesis of the TbPc$_2$ SIM at room temperature on Ag(111). These molecules show the same magnetic properties as their *ex vacuo* synthesized twins and exhibit magnetic hysteresis at 3 K. The metalation reaction is further evidenced by XPS, where exposure of 2H-Pc/Ag(111) to Tb at room temperature leads to a decrease of the NH components and the emergence of a N–Tb component at 398.1 eV. STM shows that the deposition at room temperature leads to a random distribution of double deckers. Annealing to 570 K for 30 min promotes long range diffusion of the *on-surface* synthesized double deckers, leading to large-scale ordered islands, very similar to those observed for *ex vacuo* synthesized TbPc$_2$/Ag(100). We show the robustness of the magnetic properties of TbPc$_2$/Ag(111) towards exposure to air. Moreover, we demonstrate the *on-surface* synthesis of Tb(tbu-Pc)$_2$/Ag(111) which is the first solely on-surface synthesized single-ion magnet exhibiting magnetic hysteresis when in direct contact with a metal surface. The successful *on-surface* synthesis of TbPc$_2$ and Tb(tbu-Pc)$_2$ thus opens a promising route for creating novel rare-earth based single ion magnets.

Methods

Sample preparation

The Ag(111) single crystal was cleaned by repeated cycles of sputtering with Ar$^+$ ions and annealing to 750–770 K. 2H-Pc and tbu-2H-Pc molecules were obtained from Sigma Aldrich with 98% and 85% purity respectively. The molecules were sublimed from a thermally heated quartz crucible (2H-Pc at 570 K and tbu-2H-Pc at 590 K) onto the substrate maintained at room temperature. One ML of 2H-Pc molecules is defined as one complete close-packed layer in direct contact with the substrate. The Tb coverage was determined from the XAS area at the Tb M$_{4,5}$ edges, based on another rare-earth metal reference (Er on Pt).[8,41] Here, one ML of Tb refers to the ideal coverage of one Tb atom per first-layer 2H-Pc molecule. Therefore, one ML of

synthesized $TbPc_2$ implies two ML of 2H-Pc. We used the XLD area at the N K-edge of a sub-monolayer of *ex vacuo* synthesized $TbPc_2$ molecules, where the Tb to N ratio is defined by the molecular structure, to determine the corresponding amount of 2H-Pc molecules. The use of the XLD allows to get rid of the dominant background over the weak XAS N K-edge signal.

Tb $M_{4,5}$-edge XAS/XMCD/XLD

The X-ray absorption spectra were measured at the EPFL/PSI X-Treme beamline[42] of the Swiss Light Source and at the beamline ID32 of the European Synchrotron Radiation Facility by recording the sample drain current in total electron yield mode. Measurement settings were the same as those reported in ref. 8. The amount of deposited 2H-Pc modifies the Tb $M_{4,5}$ background. Therefore, in order to compare the data obtained from samples with varied 2H-Pc coverage measured during different experimental sessions, we subtracted a polynomial profile and obtained a flat background for all energies apart from the M_5 and M_4 peak regions. All spectra are normalized to the total XAS defined as the total absorption $\sigma_+ + \sigma_-$ for circular polarizations and $\sigma_v + \sigma_h$ for linear polarizations.

XPS

The XPS data were recorded at the ALOISA beamline at Elettra. The molecular coverage was controlled *via* a quartz microbalance where the deposition parameters were known from other tetrapyrrole experiments performed at this beamline.[43,44] The N 1s spectra were recorded at a photon energy of 500 eV. The energy scale was calibrated against the Ag $3d_{5/2}$ line at 386.3 eV. Spectra of the Ag 3d region were measured each time directly after the acquisition of N 1s spectra.[45] Shirley background was subtracted from all raw data. Fitting of the N 1s region was done using Gaussian curves to avoid the introduction of additional free parameters in Voigt curves. Quantitative analysis from such fitting is complicated since even for the unreacted 2H-Pc molecules on a perfectly subtracted background, the spectrum should be fitted with at least four peaks, (a) the pyrrolic (NH) species (green), (b) the iminic (central N) species (blue), (c) the aza (outer N) species (blue), and (d) the shake-up peak. For metalated molecules additional three peaks should be included: (a) the metal coordinated species (N–Tb) (orange), (b) the aza (outer N) species, and (c) the shake-up peak. In principle, this number should be doubled due to different first and second layer contributions. As using such a large amount of peaks would overdetermine the available data, and to ensure comparability with the results from the literature,[28,46] the spectra in Fig. 2a were fitted with three or five peaks. The underlying assumptions are as follows: (i) the 0.1–0.2 eV shift[46] between first and second layer is neglected and (ii) the shift of 0.35 eV (ref. 47) between iminic and aza nitrogen atoms is neglected for both 2H-Pc as well as for $TbPc_2$.

The top panel of Fig. 2a includes three components: the N, NH, and a shake-up peak of the main peak N. This shake-up peak has 2% of the total area and the total contribution from peak N (combined intensity of N and its shake-up) is constrained to be three times that of the NH peak, following

stoichiometry. For the metalated case (Fig. 2b), we have introduced two additional components, namely N–Tb and its shake up. For the metalated molecules, best fit was obtained when the combined shake-up area was 4% of the total area. For a given set of data, the FWHM were required to be the same for all species.

From the XPS fits, we obtained the total area under the N, NH, and N–Tb peak. We use this information to extract the Tb coverage. Defining α as the fraction of the free-base 2H-Pc that forms double deckers, we deduce $\alpha = \dfrac{\Delta(N-Tb)}{2\Delta(N-H) + \Delta(N-Tb)}$, following stoichiometry. Here Δ defines the area under the corresponding peak. Finally the coverage of the formed double deckers (and therefore that of deposited Tb) is calculated as $\alpha S/2$, where S is the amount of free-base deposited on Ag(111) in ML. For the lower panel in Fig. 2a, $\alpha = 0.53$.

STM

The STM images were recorded in constant current mode at 5 K using a W tip.[48] STM images of *on-surface* synthesized $TbPc_2$ on Ag(111) were acquired for samples with different coverages of 2H-Pc molecules and Tb atoms. Bias voltages indicated in the figure captions correspond to the sample potential. For the STM measurements, we first calibrated the Tb coverage by depositing Tb directly on Ag(111) and determining the covered area. The proportion of observed metalated molecules follows from this calibration.

Conflicts of interest

There are no conflicts to declare.

Acknowledgements

Notes and references

1 N. Ishikawa, M. Sugita, T. Ishikawa, S. Koshihara and Y. Kaizu, Lanthanide Double-Decker Complexes Functioning as Magnets at the Single-Molecular Level, *J. Am. Chem. Soc.*, 2003, **125**, 8694–8695, DOI: 10.1021/ja029629n.

2 N. Ishikawa, M. Sugita, T. Ishikawa, S. Koshihara and Y. Kaizu, Mononuclear Lanthanide Complexes with a Long Magnetization Relaxation Time at High Temperatures: A New Category of Magnets at the Single-Molecular Level, *J. Phys. Chem. B*, 2004, **108**, 11265–11271, DOI: 10.1021/jp0376065.

3 M. Affronte, F. Troiani, A. Ghirri, A. Candini, M. Evangelisti, V. Corradini, S. Carretta, P. Santini, G. Amoretti, F. Tuna, G. Timco and R. E. P. Winpenny, Single molecule magnets for quantum computation, *J. Phys. D: Appl. Phys.*, 2007, **40**, 2999–3004, DOI: 10.1088/0022-3727/40/10/S01.

4 S. Stepanow, J. Honolka, P. Gambardella, L. Vitali, N. Abdurakhmanova, T.-C. Tseng, S. Rauschenbach, S. L. Tait, V. Sessi, S. Klyatskaya, M. Ruben and K. Kern, Spin and Orbital Magnetic Moment Anisotropies of Monodispersed Bis(Phthalocyaninato)Terbium on a Copper Surface, *J. Am. Chem. Soc.*, 2010, **132**, 11900–11901, DOI: 10.1021/ja105124r.

5 R. Vincent, S. Klyatskaya, M. Ruben, W. Wernsdorfer and F. Balestro, Electronic read-out of a single nuclear spin using a molecular spin transistor, *Nature*, 2012, **488**, 357–360, DOI: 10.1038/nature11341.

6 S. Thiele, F. Balestro, R. Ballou, S. Klyatskaya, M. Ruben and W. Wernsdorfer, Electrically driven nuclear spin resonance in single-molecule magnets, *Science*, 2014, **344**, 1135–1138, DOI: 10.1126/science.1249802.

7 J. Dreiser, Molecular lanthanide single-ion magnets: from bulk to submonolayers, *J. Phys.: Condens. Matter*, 2015, **27**, 183203, DOI: 10.1088/0953-8984/27/18/183203.

8 C. Wäckerlin, F. Donati, A. Singha, R. Baltic, S. Rusponi, K. Diller, F. Patthey, M. Pivetta, Y. Lan, S. Klyatskaya, M. Ruben, H. Brune and J. Dreiser, Giant Hysteresis of Single-Molecule Magnets Adsorbed on a Nonmagnetic Insulator, *Adv. Mater.*, 2016, **28**, 5195–5199, DOI: 10.1002/adma.201506305.

9 C. A. P. Goodwin, F. Ortu, D. Reta, N. F. Chilton and D. P. Mills, Molecular magnetic hysteresis at 60 kelvin in dysprosocenium, *Nature*, 2017, **548**, 439–442, DOI: 10.1038/nature23447.

10 F.-S. Guo, B. M. Day, Y.-C. Chen, M.-L. Tong, A. Mansikkamäki and R. A. Layfield, A Dysprosium Metallocene Single-Molecule Magnet Functioning at the Axial Limit, *Angew. Chem., Int. Ed.*, 2017, **56**, 1–6, DOI: 10.1002/anie.201705426.

11 K. Katoh, Y. Yoshida, M. Yamashita, H. Miyasaka, B. K. Breedlove, T. Kajiwara, S. Takaishi, N. Ishikawa, H. Isshiki, Y. F. Zhang, *et al.*, Direct Observation of Lanthanide(III)-Phthalocyanine Molecules on Au(111) by Using Scanning Tunneling Microscopy and Scanning Tunneling Spectroscopy and Thin-Film Field-Effect Transistor Properties of Tb(III)- and Dy(III)-Phthalocyanine Molecules, *J. Am. Chem. Soc.*, 2009, **131**, 9967–9976, DOI: 10.1021/ja902349t.

12 L. Malavolti, V. Lanzilotto, S. Ninova, L. Poggini, I. Cimatti, B. Cortigiani, L. Margheriti, D. Chiappe, E. Otero, P. Sainctavit, F. Totti, A. Cornia, M. Mannini and R. Sessoli, Magnetic Bistability in a Submonolayer of Sublimated Fe₄ Single-Molecule Magnets, *Nano Lett.*, 2015, **15**, 535–541, DOI: 10.1021/nl503925h.

13 E. Kiefl, M. Mannini, K. Bernot, X. Yi, A. Amato, T. Leviant, A. Magnani, A. Prokscha, T. Suter, R. Sessoli and Z. Salman, Robust Magnetic Properties of a Sublimable Single-Molecule Magnet, *ACS Nano*, 2016, **10**, 5663–5669, DOI: 10.1021/acsnano.6b01817.

14 J. Dreiser, G. E. Pacchioni, F. Donati, L. Gragnaniello, A. Cavallin, K. S. Pedersen, J. Bendix, M. Delley, B. Pivetta, S. Rusponi and H. Brune, Out-of-Plane Alignment of Er(trensal) Easy Magnetization Axes Using Graphene, *ACS Nano*, 2016, **10**, 2887–2892, DOI: 10.1021/acsnano.5b08178.

15 S. Kahle, Z. Deng, N. Malinowski, C. Tonnoir, A. Forment-Aliaga, N. Thontasen, G. Rinke, D. Le, V. Turkowski, T. S. Rahman, S. Rauschenbach, M. Ternes and K. Kern, The Quantum Magnetism of Individual Manganese-12-Acetate Molecular Magnets Anchored at Surfaces, *Nano Lett.*, 2012, **12**, 518–521, DOI: 10.1021/nl204141z.

16 L. Gragnaniello, F. Paschke, P. Erler, P. Schmitt, N. Barth, S. Simon, H. Brune, S. Rusponi and M. Fonin, Uniaxial 2D Superlattice of Fe₄ Molecular Magnets on Graphene, *Nano Lett.*, 2017, **17**, 7177–7182, DOI: 10.1021/acs.nanolett.6b05105.

17 K. Diller, A. C. Papageorgiou, F. Klappenberger, F. Allegretti, J. V. Barth and W. Auwärter, In vacuo interfacial tetrapyrrole metallation, *Chem. Soc. Rev.*, 2016, **45**, 1629–1656, DOI: 10.1039/c5cs00207a.

18 J. M. Gottfried, Surface chemistry of porphyrins and phthalocyanines, *Surf. Sci. Rep.*, 2015, **70**, 259–379, DOI: 10.1016/j.surfrep.2015.04.001.

19 H. Marbach, Surface-Mediated in Situ Metalation of Porphyrins at the Solid – Vacuum Interface, *Acc. Chem. Res.*, 2015, **48**, 2649–2658, DOI: 10.1021/acs.accounts.5b00243.

20 J. M. Gottfried, K. Flechtner, A. Kretschmann, T. Lukasczyk and H.-P. Steinrück, Direct Synthesis of a Metalloporphyrin Complex on a Surface, *J. Am. Chem. Soc.*, 2006, **128**, 5644–5645, DOI: 10.1021/ja0610333.

21 T. E. Shubina, H. Marbach, K. Flechtner, A. Kretschmann, N. Jux, F. Buchner, H. Steinrück, T. Clark and J. M. Gottfried, Principle and Mechanism of Direct Porphyrin Metalation: Joint Experimental and Theoretical Investigation, *J. Am. Chem. Soc.*, 2007, **129**, 9476–9483, DOI: 10.1021/ja072360t.

22 M. Nardi, R. Verucchi, R. Tubino and S. Iannotta, Activation and control of organolanthanide synthesis by supersonic molecular beams: Erbium-porphyrin test case, *Phys. Rev. B: Condens. Matter Mater. Phys.*, 2009, **79**, 125404–125409, DOI: 10.1103/PhysRevB.79.125404.

23 A. Weber-Bargioni, J. Reichert, A. P. Seitsonen, W. Auwärter, A. Schiffrin and J. V. Barth, Interaction of Cerium Atoms with Surface-Anchored Porphyrin Molecules, *J. Phys. Chem. C*, 2008, **112**, 3453–3455, DOI: 10.1021/jp076961i.

24 F. Bischoff, K. Seufert, W. Auwärter, A. P. Seitsonen, D. Heim and J. V. Barth, Metalation of Porphyrins by Lanthanide Atoms at Interfaces: Direct Observation and Stimulation of Cerium Coordination to 2H-TPP/Ag(111), *J. Phys. Chem. C*, 2018, **122**, 5083–5092, DOI: 10.1021/acs.jpcc.7b10363.

25 D. Écija, W. Auwärter, S. Vijayaraghavan, K. Seufert, F. Bischoff, K. Tashiro and J. V. Barth, Assembly and Manipulation of Rotatable Cerium Porphyrinato Sandwich Complexes on a Surface, *Angew. Chem., Int. Ed.*, 2011, **50**, 3872–3877, DOI: 10.1002/anie.201007370.

26 G. Serrano, E. Velez-Fort, I. Cimatti, B. Cortigiani, L. Malavolti, D. Betto, A. Ouerghi, N. B. Brookes, M. Mannini and R. Sessoli, Magnetic bistability of a TbPc$_2$ submonolayer on a graphene/SiC(0001) conductive electrode, *Nanoscale*, 2018, **10**, 2715, DOI: 10.1039/c7nr08372f.

27 S. Kera, M. Casu, K. Bauchspieß, D. Batchelor, T. Schmidt and E. Umbach, Growth mode and molecular orientation of phthalocyanine molecules on metal single crystal substrates: A NEXAFS and XPS study, *Surf. Sci.*, 2006, **600**, 1077–1084, DOI: 10.1016/j.susc.2005.12.042.

28 Y. Bai, F. Buchner, M. T. Wendahl, I. Kellner, A. Bayer, H.-P. Steinrück, H. Marbach and J. M. Gottfried, Direct Metalation of a Phthalocyanine Monolayer on Ag(111) with Coadsorbed Iron Atoms, *J. Phys. Chem. C*, 2008, **112**, 6087–6092, DOI: 10.1021/jp711122w.

29 Y. Alfredsson, B. Brena, K. Nilson, J. Åhlund, L. Kjeldgaard, M. Nyberg, Y. Luo, N. Mårtensson, A. Sandell, C. Puglia and H. Siegbahn, Electronic structure of a vapor-deposited metal-free phthalocyanine thin film, *J. Chem. Phys.*, 2005, **122**, 214723, DOI: 10.1063/1.1924539.

30 V. N. Nemykin, P. Galloni, B. Floris, C. D. Barrett, R. G. Hadt, R. I. Subbotin, A. G. Marrani, R. Zanoni and N. M. Loim, Metal-free and transition-metal tetraferrocenylporphyrins part 1: synthesis, characterization, electronic structure, and conformational flexibility of neutral compounds, *Dalton Trans.*, 2008, 4233–4246, DOI: 10.1039/b805156a.

31 S. Fahrendorf, N. Atodiresei, C. Besson, V. Caciuc, F. Matthes, S. Blügel, P. Kögerler, D. E. Bürgler and C. M. Schneider, Accessing 4f-states in single-molecule spintronics, *Nat. Commun.*, 2013, **4**, 2425, DOI: 10.1038/ncomms3425.

32 T. Komeda, K. Katoh and M. Yamashita, Double-decker phthalocyanine complex: Scanning tunneling microscopy study of film formation and spin properties, *Prog. Surf. Sci.*, 2014, **89**, 127–160, DOI: 10.1016/j.progsurf.2014.03.001.

33 Y. He, Y. Zhang, I.-P. Hong, F. Cheng, X. Zhou, Q. Shen, J. Li, Y. Wang, J. Jiang and K. Wu, Low-temperature scanning tunneling microscopy study of double-decker DyPc$_2$ on Pb Surface, *Nanoscale*, 2014, **6**, 10779–10783, DOI: 10.1039/C4NR02863E.

34 G. Serrano, S. Wiespointner-Baumgarthuber, S. Tebi, S. Klyatskaya, M. Ruben, R. Koch and S. Müllegger, Bilayer of Terbium Double-Decker Single-Molecule Magnets, *J. Phys. Chem. C*, 2016, **120**, 13581, DOI: 10.1021/acs.jpcc.6b03676.

35 H. Isshiki, J. Liu, K. Katoh, M. Yamashita, H. Miyasaka, B. K. Breedlove, S. Takaishi and T. Komeda, Scanning Tunneling Microscopy Investigation of Tris(phthalocyaninato)yttrium Triple-Decker Molecules Deposited on Au(111), *J. Phys. Chem. C*, 2010, **114**, 12202, DOI: 10.1021/jp101349v.

36 J. Hellerstedt, A. Cahlík, M. Švec, B. de la Torre, M. Moro-Lagares, T. Chutora, B. Papoušková, G. Zoppellaro, P. Mutombo, M. Ruben, R. Zbořil and P. Jelinek, On-surface structural and electronic properties of spontaneously formed Tb$_2$Pc$_3$ single molecule magnets, *Nanoscale*, 2018, **10**, 15553, DOI: 10.1039/c8nr04215b.

37 T. Komeda, H. Isshiki, J. Liu, Y.-F. Zhang, N. Lorente, K. Katoh, B. K. Breedlove and M. Yamashita, Observation

and electric current control of a local spin in a single-molecule magnet, *Nat. Commun.*, 2011, **2**, 217, DOI: 10.1038/ncomms1210.

38 Z. Deng, S. Rauschenbach, S. Stepanow, S. Klyatskaya, M. Ruben and K. Kern, Self-assembly of bis(phthalocyaninato)terbium on metal surfaces, *Phys. Scr.*, 2015, **90**, 098003, DOI: 10.1088/0031-8949/90/9/098003.

39 Z. T. Deng, H. M. Guo, W. Guo, L. Gao, Z. H. Cheng, D. X. Shi and H.-J. Gao, Structural Properties of Tetra-tert-butyl Zinc(II) Phthalocyanine Isomers on a Au(111) Surface, *J. Phys. Chem. C*, 2009, **113**, 11223–11227, DOI: 10.1021/jp901193h.

40 V. N. Nemykin and E. A. Lukyanets, Synthesis of substituted phthalocyanines, *Arkivoc*, 2010, **2010**, 136, DOI: 10.3998/ark.5550190.0011.104.

41 A. Singha, R. Baltic, F. Donati, C. Wäckerlin, J. Dreiser, L. Persichetti, S. Stepanow, P. Gambardella, S. Rusponi and H. Brune, 4f occupancy and magnetism of rare-earth atoms adsorbed on metal substrates, *Phys. Rev. B*, 2017, **96**, 224418, DOI: 10.1103/PhysRevB.96.224418.

42 C. Piamonteze, U. Flechsig, S. Rusponi, J. Dreiser, J. Heidler, M. Schmidt, R. Wetter, M. Calvi, T. Schmidt, H. Pruchova, J. Krempasky, C. Quitmann, H. Brune and F. Nolting, X-Treme beamline at SLS: X-ray magnetic circular and linear dichroism at high field and low temperature, *J. Synchrotron Radiat.*, 2012, **19**, 661, DOI: 10.1107/S0909049512027847.

43 L. Floreano, A. Cossaro, R. Gotter, A. Verdini, G. Bavdek, F. Evangelista, A. Ruocco, A. Morgante and D. Cvetko, Periodic Arrays of Cu-Phthalocyanine Chains on Au(110), *J. Phys. Chem. C*, 2008, **112**, 10794–10802, DOI: 10.1021/jp711140e.

44 G. Di Santo, C. Castellarin-Cudia, M. Fanetti, B. Taleatu, P. Borghetti, L. Sangaletti, L. Floreano, E. Magnano, F. Bondino and A. Goldoni, Conformational Adaptation and Electronic Structure of 2H-Tetraphenylporphyrin on Ag(111) during Fe Metalation, *J. Phys. Chem. C*, 2011, **115**, 4155–4162, DOI: 10.1021/jp111151n.

45 A. Thompson, D. Attwood, E. Gullikson, M. Howells, K.-J. Kim, J. Kirz, J. Kortright, I. Lindau, Y. Liu, P. Pianetta, A. Robinson, J. Scofield, J. Underwood and G. Wiliams, *X-ray data booklet*, Lawrence Berkeley National Laboratory, University of California, 3rd edn, 2009.

46 K. Eguchi, T. Nakagawa, Y. Takagi and T. Yokoyama, Direct Synthesis of Vanadium Phthalocyanine and Its Electronic and Magnetic States in Monolayers and Multilayers on Ag(111), *J. Phys. Chem. C*, 2015, **119**, 9805–9815, DOI: 10.1021/jp512935v.

47 L. Ottaviano, L. Lozzi, F. Ramondo, P. Picozzia and S. Santucci, Copper hexadecafluoro phthalocyanine and naphthalocyanine: The role of shake up excitations in the interpretation and electronic distinction of high-resolution X-ray photoelectron spectroscopy measurements, *J. Electron Spectrosc. Relat. Phenom.*, 1999, **105**, 145–154, DOI: 10.1016/S0368-2048(99)00064-X.

48 R. Gaisch, J. K. Gimzewski, B. Reihl, R. R. Schlittler, M. Tschudy and W. D. Schneider, Low-temperature ultra-high-vacuum scanning tunneling microscope, *Ultramicroscopy*, 1992, **1621**, 42–44, DOI: 10.1016/0304-3991(92)90495-6.